All-Optical Parametric-Assisted Oversampling and Decimation for Signal Denoising Amplification

Manuel P. Fernandez,* Saket Kaushal, Benjamin Crockett, Laureano A. Bulus-Rossini, Pablo A. Costanzo-Caso, and José Azaña

Decimation is a common process in digital signal processing that involves reducing the sampling rate of an oversampled signal by linearly combining consecutive samples. Among other applications, this process represents a simple means to mitigate noise content in the digital signal. In this work, a novel optical signal processing concept inspired by these operations is proposed, which is called *Parametric-assisted Oversampling and Decimation* (POD). By using a simple all-fiber setup, the POD processor first realizes an ultra-fast parametric oversampling of the incoming temporal signal (at >100 Gigasamples per second), a process that is followed by a decimation that reduces the sampling rate by any user-defined factor in a lossless manner. In this way, the POD delivers an amplified sampled copy of the optical signal, where the peak-to-peak gain results from the combination of parametric amplification and a "passive" amplification equal to the decimation factor. In this report, joint parametric and passive amplification by a factor ≈50 on GHz-bandwidth signals is demonstrated. Furthermore, it is shown that the decimation process can effectively mitigate effects of narrowband noise, outperforming traditional optical and digital filtering techniques. By experimentally achieving ultra-high decimation factors (>750), narrowband (MHz-bandwidth) optical waveformsthat are lost in a much stronger noise background are recovered.

1. Introduction

Accurate detection of temporal optical signals is fundamental in numerous scientific and engineering fields, and the features of the signal to be detected, in terms of its temporal

dynamics, change significantly depending on the application. For instance, detection of broadband optical signals (with bandwidths > 10 GHz) is required in modern lightwave telecommunication systems,[1] real-time spectroscopy[2,3] and microwave photonics.[4,5] On the other hand, narrowband optical signals (with bandwidths < 1 GHz) are found in applications like biomedical imaging[6] and radio-astronomy.[7] In sensing and ranging applications like LiDARs[8] and optical time-domain reflectometry,[9] the receivers need to acquire extremely weak backscattered signals with bandwidths spanning from the MHz to the GHz regime, depending on the target resolution. Regardless of the particular requirements of each application, all of them have in common that their performance hinges on the ability to acquire temporal optical waveforms with the highest fidelity possible. In this respect, one of the major obstacles to the measurement accuracy is noise superposed to the expected waveform, causing undesired random fluctuations in the amplitude and phase of the complex electric field. This is particularly challenging when dealing with weak signals (e.g., with powers below the detection threshold), a common situation in many of the aforementioned applications.

In such a case, optical amplifiers like Erbium-doped fiber amplifiers (EDFAs) provide simple and robust platforms to increase the intensity of the signal to a desired level through an active gain process, making the measurement ultimately limited by optical noise over noises of electronic origin.[10] Recently, fiber-optic parametric amplifiers (FOPAs) based on four-wave mixing (FWM) have attracted a great deal of attention due to their unique features, including extremely high gains (up to 70 dB demonstrated),[11,12] broadband gain spectra that can extend beyond 100 nm[13,14] and the flexibility to operate in different wavelength bands. Additionally, since the FWM process has very fast energy transitions, a proper design of the pump signal can simultaneously offer functionalities like wavelength conversion,[15–17] all-optical sampling[18] and the realization of time-lenses for several signal processing applications.[19,20] However, in every amplification system, besides the injection of additional undesired noise (e.g., through amplified spontaneous

M. P. Fernandez, S. Kaushal, B. Crockett, J. Azaña
Institut National de la Recherche Scientifique – Centre Énergie Matériaux Télécommunications
Montréal, QC H5A 1K6, Canada
E-mail: manuel.fernandez@inrs.ca

M. P. Fernandez, L. A. Bulus-Rossini, P. A. Costanzo-Caso
Laboratorio de Investigación Aplicada en Telecomunicaciones - Instituto Balseiro (UNCuyo-CNEA) & CONICET
Bariloche, RN 8400, Argentina

emission, ASE), both the signal and the pre-existent noise are simultaneously amplified,[21] unavoidably worsening the accuracy of the subsequent signal measurement. In fact, noise-free amplification still remains to be an asymptotic value reserved to phase-sensitive parametric amplifiers.[22,23] Furthermore, parametric amplifiers have a limitation where the gain they produce depends on the amount of pump power that is coupled into the nonlinear medium. In this way, apart from the need for high power optical sources, with increasing pump powers other undesired nonlinear effects start to be relevant and limit the achievable gain. These effects include cross-gain modulation, nonlinear crosstalk,[24] stimulated Brillouin scattering,[25] and nonlinear absorption.[26]

When it comes to noise mitigation, the optical band-pass filter (BPF) is the preferred solution to remove out-of-band noise (i.e., noise that is outside the frequency band of the signal of interest). However, in order to use a BPF, previous knowledge of the incoming signal's central frequency and bandwidth is a must, and these parameters are not always known or even may change in time. For instance, the signal's central frequency can change due to thermal instabilities of the lasers, interactions with acoustic waves, Doppler effect, etc. Moreover, most of commercial BPFs do not offer bandwidths below just a few GHz, and thus they are a sub-optimal solution for narrowband optical signals with bandwidths of a few MHz or narrower. A wide variety of technologies have been proposed to realize narrowband optical filters,[27–30] but all of them still face the above-mentioned difficulties concerning the need for a precise and stable frequency alignment. Alternatively, coherent detection followed by narrowband filtering in the digital domain is widely employed in applications like modern communication systems.[31] However, this approach still requires a very precise alignment between the incoming signal and a local oscillator. When considering the signal after photodetection, one may resort to temporal averaging to reduce the effect of some noise contributions,[32] but this procedure is unsuited for the measurement of the non-repetitive signals often found across many practical applications. Additionally, some noise contributions in the detected signal, like the ASE-ASE beat noise, have non-zero mean value and, thus, they cannot be removed through averaging.[10] In conclusion, the accurate detection of optical signals corrupted by noise is a relevant problem for a myriad of applications, and still remains unsolved under many practical conditions.

Alternatively, we have recent proposals for denoising passive amplification of optical signals exploiting Talbot effects. The so-called Talbot amplifier was first proposed for passive amplification of periodic waveforms,[33,34] in which a suitable temporal phase modulation followed by group-velocity dispersion (GVD) redistribute the energy of the signal into a replica of itself with a repetition period and peak power both multiplied by an integer factor, q. Later, the concept was extended to continuous non-periodic signals in a system that is known as temporal Talbot array illuminator (T-TAI).[35–37] Here, similar phase-only operations are used to focus the coherent content of the input signal into periodic short pulses outlining an amplified copy of the signal, whereas the stochastic (non-coherent) noise remains nearly unaltered.[37] For their practical implementation, Talbot-based amplifiers need to realize a sophisticated temporal phase modulation in discrete short time-bins of length T/q, with q being

the target amplification factor and T being the output sampling period. Thus, this design is specifically suited for implementation using electro-optic phase modulation driven by a high-speed arbitrary waveform generation, where the finite bandwidth of the electronics imposes a fundamental limit on the maximum bandwidth of the input signal, since T needs to be low enough to comply with the Nyquist sampling theorem. Additionally, for a prescribed sampling period, the limited modulation speed also represents a constraint on the achievable amplification (q). For instance, in previous demonstrations of Talbot amplifiers, the product (sampling rate)×(passive amplification factor) has been limited to ≈38 GHz.[37]

In this work, we present a novel photonic signal processing concept, which is here applied to the simultaneous denoising and amplification of arbitrary optical signals. We refer to this method as *Parametric-assisted Oversampling and Decimation* (POD). The POD processor first performs an ultra-fast optical sampling enabled by parametric FWM, a process that is followed by a lossless optical decimation (i.e., downsampling) that effectively suppresses noise-induced fluctuations in the oversampled signal while simultaneously magnifying its peak power by an amount equal to the decimation factor. As it is discussed below, this methodology can be regarded as the optical counterpart of the widely employed oversampled analog-to-digital converters (ADCs),[38,39] where the oversampling process allows to relax the specifications of analog anti-aliasing filters, while the mitigation of the noise content in the signal is realized through a sample decimation in the digital domain. In this way, the POD processor delivers a noise-mitigated sampled copy of the signal of interest, whose amplitude is the result of a combined parametric amplification (through FWM) and a passive amplification (through a lossless decimation process). The ultra-fast optical oversampling and the decimation processes are enabled by suitable dispersive propagations according to the fractional Talbot effect. We experimentally demonstrate integer (even and odd) as well as fractional decimation factors. The all-optical nature of the POD enables the realization of ultra-high oversampling rates and passive amplification (decimation) factors. In this work, we report a (sampling rate)×(passive amplification factor) product exceeding 380 GHz, more than one order of magnitude improvement versus electro-optic Talbot amplifiers. By achieving an ultra-high decimation factor of 764.5, we show the recovery of weak optical signals completely buried in a noisy background, where a conventional detection scheme is fairly insufficient.

2. Concept and Operation Principle

In this section, we first conceptually describe the principle of the proposed optical oversampling-and-decimation process. Then, we describe its practical implementation using parametric FWM, which yields to the POD itself.

2.1. Oversampling and Decimation Through Temporal Talbot Effects

The proposed oversampling-and-decimation is based on the temporal Talbot effect, a self-imaging process that occurs when a periodic pulse train propagates in a group-velocity dispersive
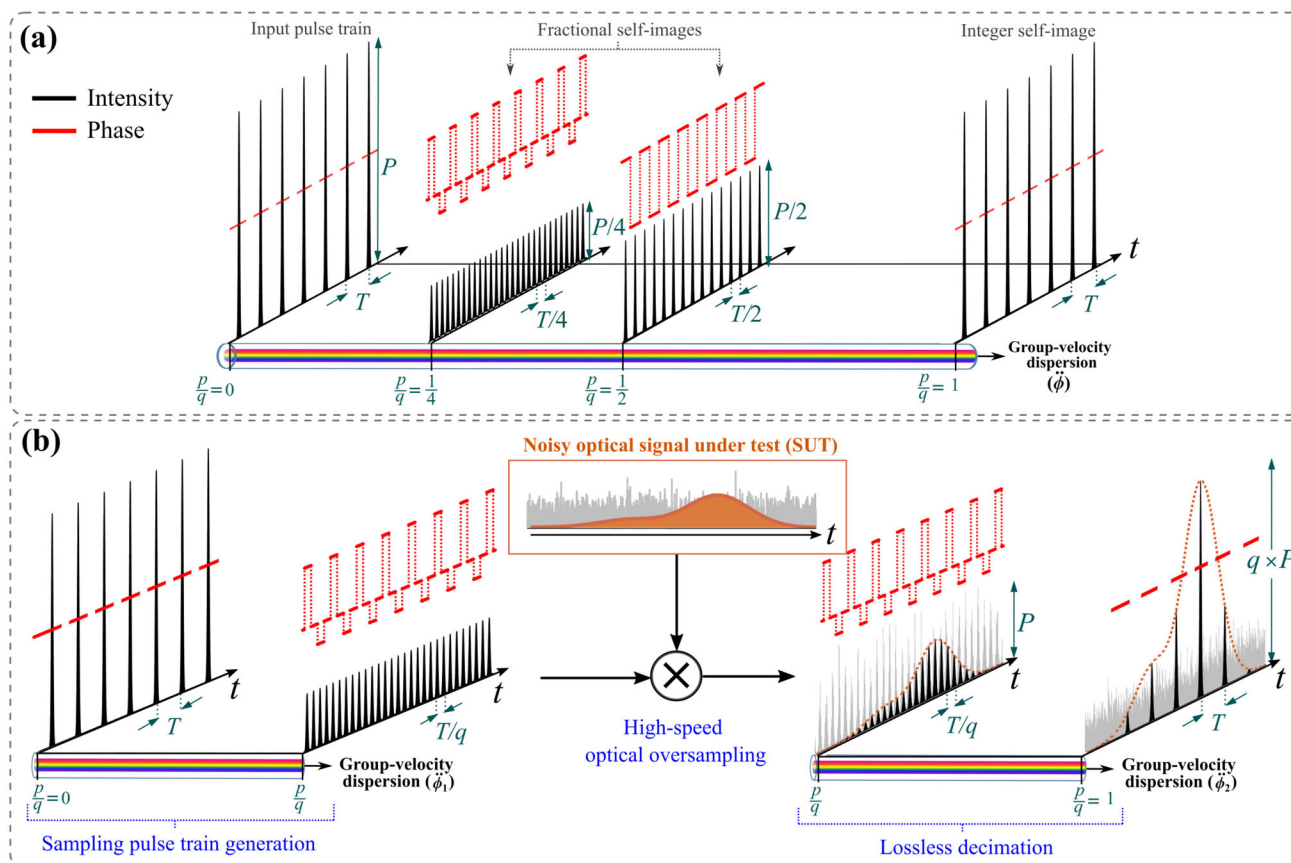
Figure 1. Optical oversampling and decimation based on the Talbot effect. a) The standard temporal Talbot effect, where the input pulse train is perfectly restored when $p/q = 1$ in Equation 1 (i.e., at an integer Talbot distance), while fractional self-images are formed as long as p/q is a rational number. b) Proposed denoising passive amplification of arbitrary waveforms through oversampling and decimation. The noisy SUT is first sampled by a high-speed pulse train after self-imaging of order q. The subsequent dispersive propagation of the oversampled SUT to the closest integer Talbot distance reduces the sampling rate while increasing the amplitude of the samples by a factor q.

medium.[40,41] As illustrated in **Figure 1**a, a T-periodic pulse train is perfectly restored after a specific GVD propagation, yielding to what is known as an integer self-image of the input pulse train. More interestingly, the interaction between consecutive dispersed pulses interfering with each other yields to the formation of fractional self-images, which are exact copies of the input pulse train presenting a repetition rate that is multiplied by an arbitrary integer factor and whose peak intensity is divided by the same amount. Specifically, in order to multiply the repetition rate by a factor q, the GVD parameter $\ddot{\phi}$ (slope of the group delay vs radial frequency) must satisfy[41–44]
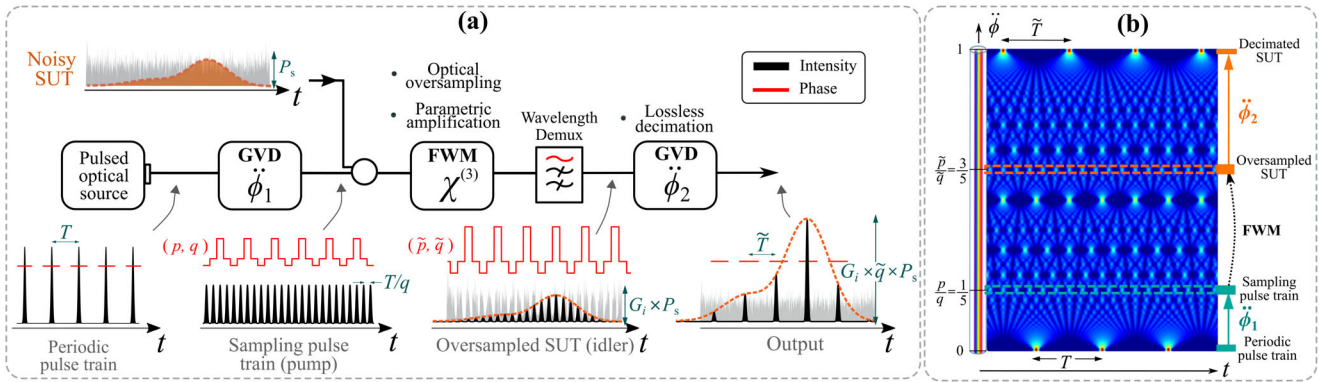
$$\ddot{\phi} = \sigma \frac{p}{q} \frac{T^2}{2\pi} \tag{1}$$

with p and q being two co-prime natural numbers, such that p/q is a rational number, and $\sigma = \pm 1$ defining the sign of the dispersion. All of the possible sets (p, q) form the so-called Talbot carpet, where each rate-multiplied self-image is affected by a deterministic pulse-to-pulse quadratic temporal phase structure,[42,44] as shown in Figure 1a for $q = 2$ and $q = 4$.

Our proposal exploits these concepts to realize an oversampling and subsequent decimation of an arbitrary optical signal

under test (SUT). The operations required to do this are illustrated in Figure 1b. First, the repetition rate of a pulse train with original period T is multiplied by an integer factor q through its propagation in a first GVD medium ($\ddot{\phi}_1$) satisfying a fractional self-imaging condition. This results in the sampling pulse train, which is a high repetition rate (>100 GHz) pulse train that additionally presents a pulse-to-pulse phase modulation in accordance with the designed fractional image, p/q. The SUT is then temporally modulated by the sampling pulse train, from which an oversampled and phase-modulated version of the SUT is obtained. Finally, a lossless optical decimation by a factor q is effectively realized by propagating the oversampled SUT to the closest integer self-image in the Talbot carpet (i.e., either to $p/q = 1$ or $p/q = 0$) through a second GVD medium ($\ddot{\phi}_2$). If passive losses in the dispersive medium are neglected, the outcome is a copy of the oversampled SUT, where the sampling period and the peak intensity are multiplied by q. Thus, the decimation factor will be also referred to as the passive amplification factor.

As it is demonstrated in Section S2 (Supporting Information), each decimated output pulse is formed as a weighted linear combination of $\approx q$ consecutive pulses of the oversampled SUT. Consequently, during the decimation process, the pulse-to-pulse random fluctuations in the oversampled SUT that occur on a

**ADVANCED
SCIENCE NEWS**

www.advancedsciencenews.com

LASER
& PHOTONICS
REVIEWS

www.lpr-journal.org

Figure 2. Working principle of the POD. a) System-level schematic, where the optical oversampling (sampling period $= T/q$) and simultaneous Talbot phase modulation are realized through FWM in a Kerr medium providing a parametric conversion gain G_i. After the second GVD stage, a decimated copy of the oversampled SUT (now with sampling period $= \tilde{T}$) is obtained, showing a peak-to-peak gain of $\approx G_i \times \tilde{q}$. b) Representation of the different signals in the Talbot carpet for a case in which the decimation factor is $\tilde{q} = 5$. Note how the oversampled SUT is located at a different fractional distance than the sampling pulse train.

time-scale faster than T (i.e., those caused by out-of-band noise) can be effectively mitigated in relation to the components of the SUT whose amplitude and phase remain approximately constant (i.e., coherent) within T. Therefore, the decimated samples present an enhancement in the signal-to-noise ratio that is proportional to q. The original continuous-time signal can be subsequently reconstructed in the digital domain with a much higher accuracy by interpolating the noise-mitigated decimated samples. In other words, the optical oversampling-and-decimation helps to mitigate the SUT's components whose frequency content is broader than $\approx 1/T$. For instance, we can have a noise-mitigation performance equivalent to ultra-narrowband MHz-bandwidth optical filters without requiring previous knowledge of the SUT's central wavelength, while also avoiding all the issues associated with frequency alignment.

Operationally, the structure of Figure 1b can be regarded as the optical analogous of the widely employed oversampled analog-to-digital converters (OS-ADC).[38,39] In OS-ADCs, the signal to be digitized is first sampled by the ADC at a rate K-times higher than the Nyquist sampling rate, with K being the oversampling factor. This oversampling relaxes the need for very selective analog anti-aliasing filters, which are often required before the ADC. The oversampling is followed by a decimation process that reduces the sampling rate by a factor K,[45,46] where the value of the decimated sample is obtained from a weighted sum of K consecutive input samples, for example, through the use of digital finite impulse response filters. During this process, the undesired random fluctuations that are faster than the signal of interest are mitigated, with higher decimation factors yielding to higher noise-mitigation performance. Thus, equivalently to OS-ADCs, the optical oversampling-and-decimation process relaxes the specifications of optical filters, that is, in regard of their bandwidth and required frequency alignment.

2.2. Parametric-Assisted Oversampling and Decimation

Figure 2a shows a system-level schematic of the POD, a simple design that exploits parametric FWM to realize the previously

Table 1. Relationship between the Talbot parameters associated to the first (p, q, T) and second $(\tilde{p}, \tilde{q}, \tilde{T})$ dispersive stages of the POD. $\mathbb{O}$: odd integer, $\mathbb{E}$: even integer.

	$q \in \mathbb{O}$	$q \in \mathbb{E}$
$\tilde{p}$	$(1 + q)p/2 \, [\mathrm{mod}\, q]$	$p \, [\mathrm{mod}\, q/2]$
$\tilde{q}$	q	$q/2$
$\tilde{T}$	T	$T/2$

described oversampling process at high speeds while simultaneously providing the feature of parametric amplification. Here, the sampling pulse train $(u_p(t))$ is used as pump and mixed with the SUT $(u_s(t))$ in a Kerr medium with nonlinear coefficient γ and length L. Due to FWM, an idler wave is created whose complex envelope is given by $u_i(t) \propto u_p^2(t)u_s^*(t)$.[47] The scale factor that relates the peak power of the idler, P_i, to that of the input SUT, P_s, is known as the parametric conversion gain, $G_i = P_i/P_s$.[48,49] Assuming perfect phase matching and operation in the small-signal regime, this gain can be approximated as $G_i \approx (\gamma L P_p)^2$, with P_p being the pump peak power.

In contrast to the conventional parametric sampling approach,[18] in the POD the sampling process is accompanied by an ultra-fast temporal phase modulation. Specifically, the pulse-to-pulse phase profile of the sampling pulse train (associated to the fractional Talbot distance p/q) is transferred to the idler multiplied by a factor two. This phase transfer is essential to achieve the subsequent decimation process, as detailed in the following. To this respect, it can be demonstrated that the resulting phase profile is also a Talbot phase, though associated to a different location in the Talbot carpet. As illustrated in Figure 2b, the oversampled SUT (idler) is now virtually located at a fractional distance $\tilde{p}/\tilde{q}$, and associated to an original pulse train with period $\tilde{T}$. The new Talbot parameters associated to the oversampled SUT $(\tilde{p}, \tilde{q}, \tilde{T})$ depend on the parity of q as per the relationships outlined in **Table 1** (see Section S1, Supporting Information, for detailed derivations). Noteworthy is the fact that if q is even, the achievable decimation factor is reduced to $q/2$

**ADVANCED
SCIENCE NEWS**

www.advancedsciencenews.com

LASER
& PHOTONICS
REVIEWS

www.lpr-journal.org

while the effective sampling rate ($\tilde{T}^{-1}$) is doubled with respect to the repetition rate of the input pulse train.

Considering these relationships, we can find the conditions to be satisfied by the two dispersive stages in order to realize the POD processes with a target output sampling period $\tilde{T}$ and a decimation by a factor $\tilde{q}$. In particular, the first dispersive stage must be designed such that it multiplies by q the repetition rate of a pulse train with period T. To do that, $\ddot{\phi}_1$ must be

$$\ddot{\phi}_1 = \sigma \frac{p}{q} \frac{T^2}{2\pi} \tag{2}$$

Then, in order to complete a decimation by a factor $\tilde{q}$, the over-sampled SUT must be propagated to the closest integer self-image in the Talbot carpet (i.e., either to $\tilde{p}/\tilde{q} = 0$ or $\tilde{p}/\tilde{q} = 1$), for which $\ddot{\phi}_2$ can take on two possible values:

$$\ddot{\phi}_2 = -\sigma \frac{\tilde{p}}{\tilde{q}} \frac{\tilde{T}^2}{2\pi} \quad | \quad \ddot{\phi}_2 = \sigma \left(1 - \frac{\tilde{p}}{\tilde{q}}\right) \frac{\tilde{T}^2}{2\pi} \tag{3}$$

In summary, if $\ddot{\phi}_1$ and $\ddot{\phi}_2$ comply with Equations 2-3, the POD processor delivers a noise-mitigated and amplified sampled copy of the input SUT, where the peak-to-peak gain of $\approx G_i \times \tilde{q}$ results from the combination of a wavelength-converting parametric amplification ($\times G_i$) and a passive amplification via a lossless decimation process ($\times \tilde{q}$).

It is important to mention that, while the GVD value described by Equation 3 implies the realization of a decimation by an integer factor $\tilde{q}$, one can properly design the second dispersive stage such as the resulting decimation factor is any fraction of $\tilde{q}$, thus realizing a passive amplification by a factor $\tilde{q}/M$ with an associated output sampling period $\tilde{T}/M$, with $M = 1, \cdots, q - 1$. In order to do this, instead of propagating the oversampled SUT to an integer distance in the Talbot carpet, $\ddot{\phi}_2$ must be designed to propagate it to another fractional distance, now of order $\tilde{q}/M$ (see Supporting Information for details). This feature, which is demonstrated in the experiments shown below, provides an important additional degree of flexibility to design the passive amplification factor and associated output sampling period by simply modifying the value of $\ddot{\phi}_2$.

Finally, we recall that the features of the idler wave generated by FWM have been exploited in numerous signal processing applications.[15–20] In fact, it is particularly interesting to note the similarity of the schematic of Figure 2 with that of conventional FWM-based temporal imaging systems.[19,20] However, the design requirements for the POD and temporal imaging systems differ significantly in terms of the GVD lines. For instance, a temporal imaging system provides a temporally scaled (magnified or compressed) copy of time-limited waveforms, whereas the POD provides a sampled and locally amplified copy of the SUT with no fundamental time restrictions, without additional temporal scaling of the waveform and with the unique noise-mitigation capabilities here described.

3. Experiment and Results

The main features of the POD were experimentally demonstrated through three different configurations providing even, odd, and fractional decimation factors of 4, 9, and 764.5 at

sampling rates of 36.3 GSa s^{-1}, 17.1 GSa s^{-1}, and 500 MSa s^{-1}, respectively. **Table 2** shows the design parameters used to realize each configuration. The experimental setup is shown in **Figure 3**. Regarding the implementation of the POD itself, the pump was synthesized from a pulse train obtained from commercial mode-locked lasers (MLL) emitting $\approx$2 ps pulses centered at 1546 nm (Pritel–Ultrafast Optical Clock for passive amplification factors of 4 and 9 and Menlo FC1500-250-ULN for 764.5). The required dispersive lines ($\ddot{\phi}_1$ and $\ddot{\phi}_2$) were obtained through standard single-mode fibers and dispersion-compensating fibers of the appropriate length. A highly-nonlinear fiber with $L = 1$ km and $\gamma = 11$ (W km)$^{-1}$ and zero-dispersion at 1546 nm was used as Kerr medium. The generated idler was recovered using an optical band-pass filter (BPF$_2$) with a broad passband, which was deliberately set to be broader than the sampled signal and noise bandwidth in order to ensure that noise contributions were not removed by this filter. The temporal waveforms shown in this report were acquired by a 500 GHz-bandwidth optical sampling oscilloscope. For the experiments, several arbitrary optical SUTs were synthesized through intensity modulation of a continuous-wave laser source emitting at λ_{cw}, where the modulator is driven by an arbitrary waveform generator (Keysight M8196A). To generate a noisy SUT, the signal of interest was combined with an amplified and filtered incoherent noise source obtained from a superluminescent diode, with its power spectral density being confined to a narrow 3-dB bandwidth (< 200 GHz). In order to prevent any polarization-dependent filtering from mitigating noise effects, a polarization filter (PF) was employed to ensure that the desired signal and unwanted noise share the same polarization state. This guarantees that both the target signal and undesired noise are affected by any polarization-dependent process equally.

3.1. Optical Sampling Features

First, observe the features of the sampled waveform delivered by the POD. Specifically, the sampling process is compared for the two first configurations listed in Table 2, representing designs providing odd ($\tilde{q} = 9$) and even ($\tilde{q} = 4$) decimation factors at high sampling rates. In both cases, the second dispersive stage was designed to achieve an integer self-image. For these two configurations, **Figure 4** depicts the temporal traces of the pulse train emitted by the MLL, the q-times rate-multiplied sampling pulse train after temporal self-imaging, and the decimated output for the case in which the input SUT is a sinusoidal intensity modulation with frequency f_{RF} over an optical carrier centered at $\lambda_{cw} = 1554$ nm. It was observed that for the odd decimation factor of 9, the output sampling rate was equal to the original repetition rate of the MLL pulse train. Contrarily, to achieve the target even decimation factor of 4, the MLL pulse train was first self-imaged by a factor $q = 2\tilde{q} = 8$. As such, in the latter case, the achieved sampling rate was twice that of the MLL repetition rate. Slight amplitude fluctuations can be observed in the sampling pulse train. They can be attributed to interference between consecutive pulses, caused by a mismatch in the used GVD with respect to the theoretical value defined in Equation 2 and by third-order dispersion (TOD). These fluctuations can be treated as an additional noise term since they will be transferred to the oversampled SUT.

Table 2. Fundamental parameters of the three different configurations used to demonstrate the concept of the POD.

Passive amplification/Decimation factor	Output sampling rate	(σ, p, q)	MLL repetition rate	First dispersion ($\ddot{\phi}_1$)	Second dispersion ($\ddot{\phi}_2$)
$\tilde{q} = 9$	17.1 GSa s^{-1}	$(-1, 7, 9)$	17.1 GHz	-423 ps^{2}rad^{-1}	-60 ps^{2}rad^{-1}
$\tilde{q} = 4$	36.3 GSa s^{-1}	$(-1, 1, 8)$	18.15 GHz	-422 ps^{2}rad^{-1}	30 ps^{2}rad^{-1}
$\tilde{q}/2 = 764.5$	500 MSa s^{-1}	$(+1, 1, 1529)$	250 MHz	1665 ps^{2}rad^{-1}	-832 ps^{2}rad^{-1}
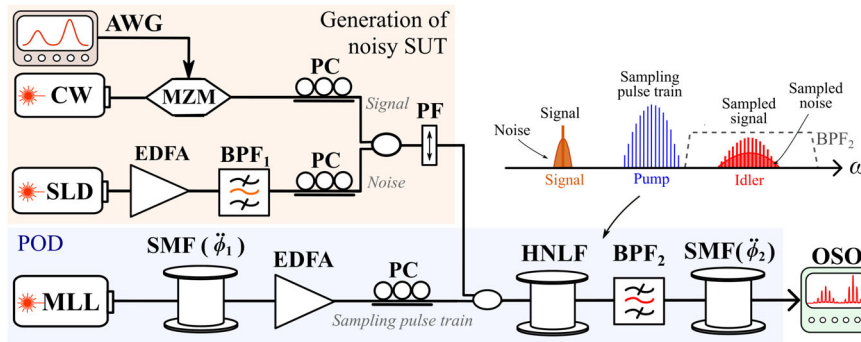
Figure 3. Experimental setup. CW: continuous-wave laser, SLD: super-luminescent diode, MLL: mode-locked laser, BPF: bandpass filter, MZM: Mach-Zehnder modulator, EDFA: Erbium-doped fiber amplifier, HNLF: highly nonlinear fiber, SMF: single mode fiber, PC: polarization controller, PF: polarization filter, OSO: optical sampling oscilloscope, AWG: arbitrary waveform generator. To ensure that the signal quality is not improved by any means other than the POD, we used PCs and a PF to align the polarization of the signal and the noise such that the parametric sampling affects them equally.

However, if the decimation factor is designed to a sufficiently high value, these minor fluctuations in the sampling pulse train will be nearly washed out and will not significantly affect the decimated output waveform. Figure 4 a3,b3 compares the output of the POD (red traces) and the associated original SUT (black dashed lines). By simple visual inspection, it is seen that an accurate sampled version of the SUT was obtained, such that the output pulse-to-pulse intensity correctly outlines the envelope of the input SUT. However, as observed in the lower traces of Figure 4 a3,b3, the sampling process becomes inaccurate when the SUT's temporal variations are as fast as the output sampling period, resulting in an aliasing effect that makes the sampled signal indistinguishable. This was similar to decimation in the digital domain. In this respect, the theoretical upper limit for the allowed SUT's fastest temporal variations is determined by the Nyquist sampling theorem, which implies that the POD sampling rate must be at least ×2 times higher than the SUT's bandwidth.

As a very important feature, the POD is inherently self-tracking in the sense that the oversampling-and-decimation process (and its associated noise-mitigation features, which are demonstrated below) is effectively realized independently of the central wavelength of the SUT. To this respect, in our experiments, we realized an accurate oversampling-and-decimation of an arbitrary SUT when its central wavelength (λ_{CW}) was swept along a span of 6 nm while maintaining the settings of the experimental setup, as it was shown in Figure S7 (Supporting Information).

3.2. Joint Parametric and Passive Amplification

Conventional parametric amplifiers provide amplification factors that are directly proportional to the squared pump power. How-

ever, with the increase of the pump power injected in the non-linear medium, other undesired nonlinear effects start to be relevant, including signal saturation, stimulated Brillouin scattering, nonlinear crosstalk resulting from spectral overlap between the pump and idler waves, and nonlinear absorption.[24–26,49] These effects can ultimately limit the maximum achievable parametric gain. To this respect, by combining the parametric amplification with a passive amplification up to a factor $\tilde{q}$ through the lossless decimation process, the POD offers an elegant solution to overcome this limitation and obtain similar levels of (peak-to-peak) signal amplification while reducing the pump peak power that needs to be coupled in the nonlinear medium. By doing so, the POD enables to achieve significant signal gain without the drawbacks associated with conventional parametric amplifiers.

This joint amplification feature was experimentally demonstrated for the aforementioned design with $\tilde{q} = 9$. In this example, an arbitrary SUT was used whose temporal profile is shown in **Figure 5**a. The measured temporal trace of the retrieved idler waveform for different values of pump power (average) is shown in Figure 5b. As expected, the created idler was an oversampled copy of the SUT, sampled at 153.9 GSa s^{-1}. As shown in the inset of Figure 5b, the measured parametric conversion gain, G_i, exhibits a quadratic dependence with the pump power, as it was expected from the theory.[48,49] In this experiment, a maximum $G_i = 8.3$ dB (i.e., an idler's peak power about ×7 times higher than that of the input SUT) was measured. In this estimation, passive losses occurring at the output bandpass filter (4 dB) and at the second dispersive fiber (1.5 dB) were not accounted for, as they could be further minimized by using optimized components. Note that, in the experiments, such passive losses were overcompensated for by the parametric gain, providing a net parametric gain of up to 2.8 dB. The associated output waveforms after lossless
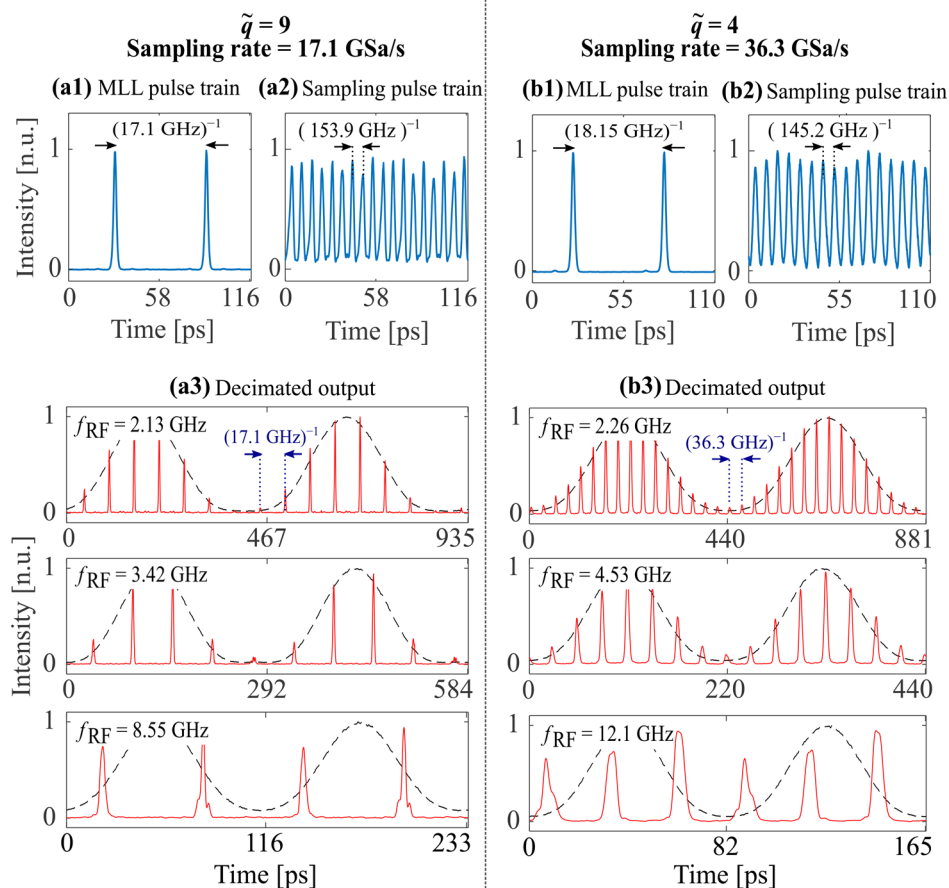
Figure 4. Sampling features of the POD processor for even and odd decimation factors. a) Decimation by a factor $\tilde{q} = 9$ and output sampling rate of 17.1 GSa s^{-1}. b) Decimation by a factor $\tilde{q} = 4$ and output sampling rate of 36.3 GSa s^{-1}. For each case, it is shown the temporal trace for (1) the original pulse train emitted by the MLL, (2) the sampling pulse train (pump) after temporal self-imaging of order q, and (3) the output of the POD corresponding to a sinusoidal SUT of increasing modulation frequencies. The intensity of the waveforms is normalized for illustration purposes.

decimation are shown in Figure 5c, where it is noted that the resulting pulse sequence outlines a faithful copy of the input SUT, now with a sampling rate reduced from 153.9 GSa s^{-1} to 17.1 GSa s^{-1}. For the evaluated pump powers, the obtained passive amplification factor, shown in the inset of Figure 5c, is estimated to range between 7.3 and 8, slightly below the designed decimation factor, which can be attributed to a residual dispersion-induced pulse broadening. This way, the measured maximum peak-to-peak amplification obtained from the combination of parametric and passive amplification was about ≈17 dB (i.e., ×50 times).

3.3. Noise Mitigation of Broadband and Narrowband Signals

In the following, the noise-mitigation capabilities of the POD processor were experimentally demonstrated by targeting the recovery of broadband and narrowband optical signals that are completely masked by ASE noise. As mentioned before, the noise content is confined to a relatively narrow bandwidth, representing a scenario in which its removal by conventional optical filters would be challenging. In this case, the reconstruction of the

SUT from the photodetected POD output was performed as follows. First, the excess of noise in the detected waveform (raw data) was removed by a digital low-pass filter with a 3-dB bandwidth $B_e = 500$ GHz, which was defined as per the expected pulse width. Then, the continuous-time SUT is reconstructed by interpolation of the detected samples. The reconstructed signal is then compared to the original noise-free SUT, where the metrics used for signal comparison are the mean-squared error (MSE) and the normalized signal amplitude (NSA), as defined in Section S3 (Supporting Information). Finally, the obtained performance in terms MSE and NSA is compared against that using the conventional signal acquisition scheme based on direct-photodetection of the noisy SUT followed by a digital low-pass filter whose bandwidth B_e matches that of the expected SUT in order to maximize noise rejection while keeping the target SUT undistorted.

First, the noise mitigation performance of the previously demonstrated design with $\tilde{q} = 9$ was demonstrated on a relatively broadband SUT, namely a 4.27 Gbps non-return to zero on-off keying (OOK) data signal centered at $\lambda_{cw} = 1536$ nm, which is shown in **Figure 6**a. This signal was then buried in a much stronger ASE noise background. Figure 6b1 shows the
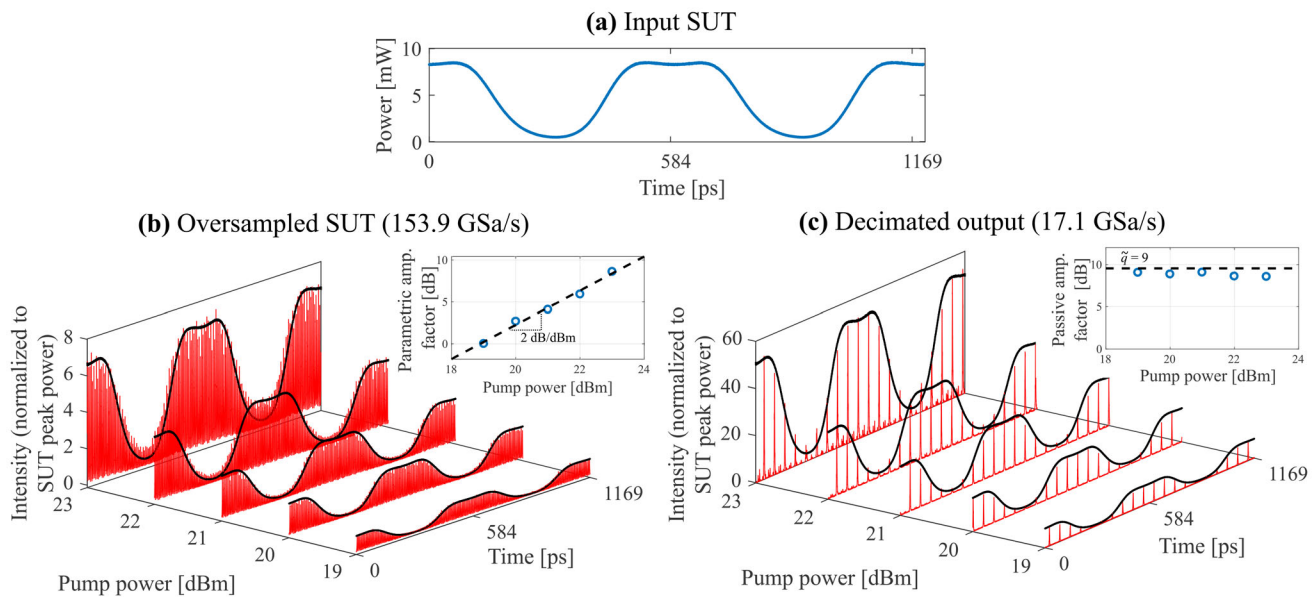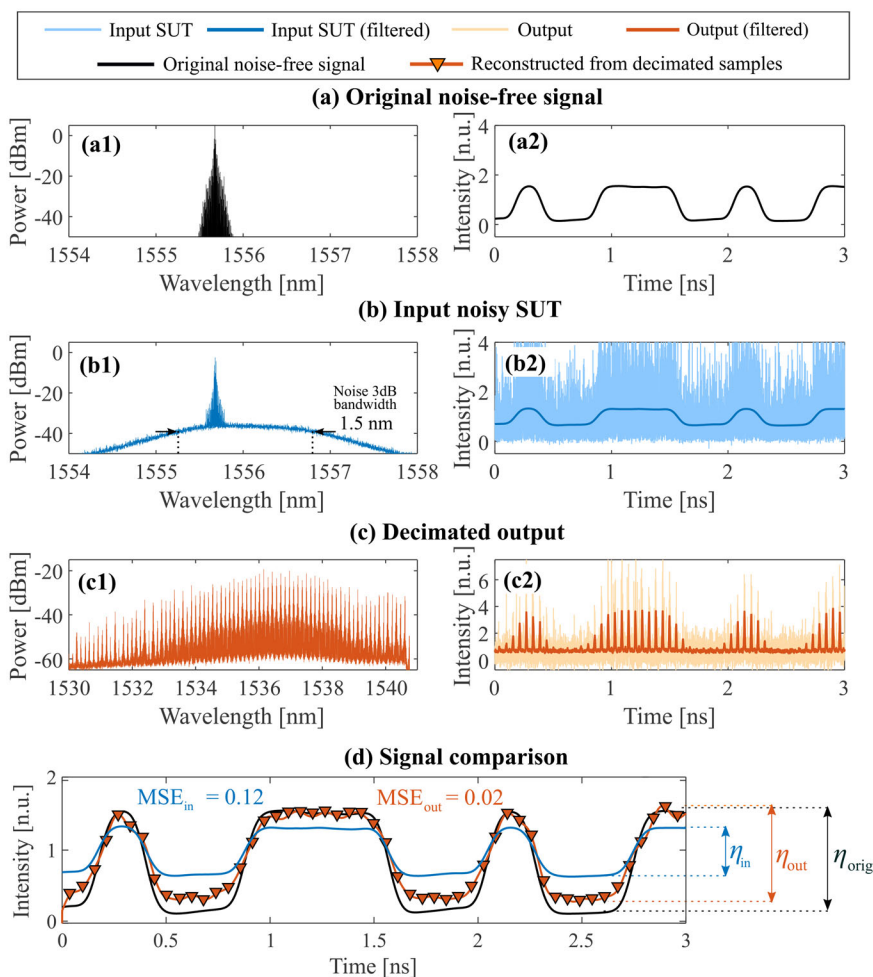
Figure 5. Measurement of combined parametric and passive amplification. a) Input SUT. b) Oversampled SUT (idler) and estimated parametric conversion gain, G_i, for increasing pump powers. As predicted by the theory, the parametric gain presents a quadratic dependence with the pump power (i.e., a slope of 2 dB/dBm). c) Decimated output of the POD for the different pump powers and estimated passive gain, which remains close to the design value ($\tilde{q} = 9$) independently of the pump power.

input noisy SUT together with its digitally low-pass filtered version. Note how the remaining in-band ASE-ASE beat noise appears as an offset that significantly reduces the extinction ratio. The spectral trace of the input noisy SUT is shown in Figure 6b2, where it is seen that the ASE noise is confined to a 3-dB bandwidth of 1.5 nm ($\approx$185 GHz), which is representative of the noise-filtering performance that can be offered by commercial narrowband optical filters. Similarly, the temporal and spectral traces of the POD output are shown in Figure 6c1,c2, respectively. It should be noted how both the signal and noise are spectrally broadened to $\approx$4 nm as a result of the sampling process. In the temporal domain, it was clearly seen how the POD output was a sampled version (17.1 GSa s^{-1}) of the input SUT. Figure 6d shows the energy-normalized temporal signals to be compared: the original noise-free SUT, the input SUT and the signal reconstructed from the POD output. It is seen how the waveform reconstructed from the POD samples shows a higher degree of similarity to the original noise-free signal than the input SUT after direct detection and optimal digital filtering. For each case, a mean-squared error with respect to the original signal of $\mathrm{MSE_{out}} = 0.02$ and $\mathrm{MSE_{SUT}} = 0.12$ was estimated. Similar improvements were obtained when analyzing the signal amplitude of the waveforms (η); for the input SUT, we measured $\mathrm{NSA_{SUT}} = 0.47$, while for the POD-reconstructed waveform, $\mathrm{NSA_{out}} = 0.84$. Thus, even for the moderate decimation factor of 9 here achieved, it was seen how the POD provides considerable improvements in terms of signal recovery.

As previously discussed, efficient noise mitigation in narrowband optical signals remains to be very challenging for conventional optical BPFs, as they typically offer pass bands above several GHz and require a precise frequency alignment with the SUT. To this respect, in order to evaluate the narrowband filtering capabilities of the POD, the recovery of a sinusoidally-

modulated signal with $f_{\mathrm{RF}} = 62.5$ MHz was targeted. In this case, the POD was designed to first oversample the SUT at the ultra-high sampling rate of 382.25 GSa s^{-1}, for which the pump was obtained from a 250 MHz pulse train that was self-imaged by a factor $q = 1529$ (yielding to $\tilde{q} = 1529$). The oversampled SUT was subsequently decimated by a fractional factor $\tilde{q}/2 = 764.5$, providing an output sampling rate of 500 MSa s^{-1}. This configuration thus provides a (sampling rate)$\times$(passive amplification factor) product of 382.25 GHz, more than one order of magnitude improvement versus previous electro-optic Talbot-based amplifiers.[37] **Figure 7** shows the temporal traces of the noisy SUT, the associated POD output and the subsequently reconstructed signal for two cases showing different optical signal-to-noise ratio (OSNR): a high-OSNR scenario (Figure 7a) and a low-OSNR scenario (Figure 7b) where the input SUT was completely buried in ASE noise. In this case, the ASE noise was spectrally confined to a bandwidth of 96 GHz, which is a representative example of the achievable performance by commercial narrowband optical filters (see Figure S4, Supporting Information, for spectral traces corresponding to this experiment). The recovered energy-normalized signals are shown in the lower part of Figure 7 where they are compared with the original noise-free SUT. Here, a remarkable performance of the POD in regard of its recovery capabilities of noise-dominated signals was observed. For instance, in the low-OSNR scenario, we observe that the input SUT presents a very low signal amplitude $\mathrm{NSA_{SUT}} = 0.19$ due to the fact that the ASE-ASE beat noise was much stronger than the target signal's amplitude. Contrarily, the signal reconstructed from the POD output is almost identical to the original SUT, and its normalized signal amplitude reaches $\mathrm{NSA_{out}} = 0.99$. Similar performance improvements in terms of signal recovery were obtained regarding the MSE, as shown in Figure 7, bottom.

**ADVANCED
SCIENCE NEWS**

www.advancedsciencenews.com

LASER
& PHOTONICS
REVIEWS

www.lpr-journal.org

Figure 6. Noise mitigation of a 4.27 Gbps OOK signal. a) Input SUT before noise loading. b) Input noisy SUT: (b1) optical spectrum and (b2) its associated detected temporal trace. c) Output of POD: (c1) optical spectrum and (c2) its associated detected temporal trace. d) Comparison of the input SUT, the recovered signal from the POD output and the original noise-free waveform. Digital low-pass filters with bandwidths $B_e = 4.27$ GHz (for the input SUT) and 500 GHz (for the POD output) are used to remove out-of-band noise in the raw detected signals.

It is worth to highlight that, in order to detect the POD output, it is generally required a much higher bandwidth than that for detecting the original SUT. Ideally, the detection bandwidth must be high enough to detect the individual pulses of the POD output without distortion. In the experiments shown in this report, the output waveforms were formed by ≈ 2 ps pulses, for which a 500 GHz-bandwidth optical sampling oscilloscope was used. However, in order to detect the non-repetitive signals often found in practice, a real-time detection scheme is needed. Therefore, for completeness, the experiments corresponding to the signal recovery of noise-dominated narrowband signals (i.e., those shown in Figure 7b) were repeated, where this time the signals were detected through a single-shot real-time acquisition scheme. Specifically, the signal acquisition consisted in a 50 GHz photodetector connected to a 28 GHz real-time oscilloscope. Temporal traces of these experiments can be found in Figure S5 (Supporting Information), where it was observed that even though the detection bandwidth is lower than the ideally required for distortion-free pulse detection, the POD still shows a greatly improved signal-recovery performance when compared

against the direct-detection scheme involving optical and digital filtering.

4. Further Discussion and Conclusion

In the following, we will delve into the practical aspects and non-idealities in the GVD stages that form the POD processor. As in any experimental implementation, the actual GVD can show deviations with respect to the theoretical values defined by Equations (2–3). In the first dispersive stage, a GVD mismatch will cause the sampling pulse train to broaden and further reduce its peak power, which directly reduces the obtained parametric conversion gain. On the other hand, a GVD mismatch in the second dispersive stage will result in residual pulse broadening of the decimated output, affecting the achieved passive amplification factor and noise-mitigation performance. In this respect, we can define a tolerance ($\Delta\ddot{\phi}$) to deviations with respect to $\ddot{\phi}_1$ and $\ddot{\phi}_2$ by using well-known metrics like the dispersion length.[50] If we set that the GVD mismatch should not exceed one dispersion length, we have that $\Delta\ddot{\phi} \leq T_0^2$, with T_0 being the half-width at $1/e$
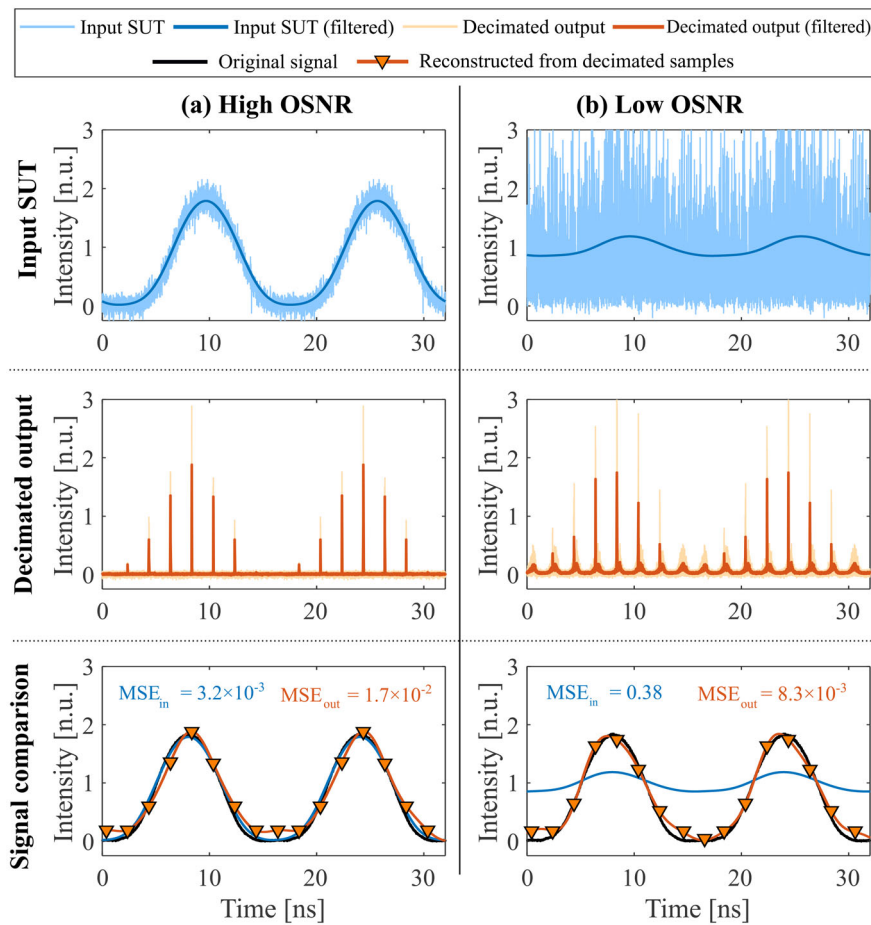
Figure 7. Noise mitigation of a narrowband signal through an ultra-high passive amplification (decimation) factor of 764.5. a) High OSNR scenario. b) Low OSNR scenario. Out-of-band noise in the photodetected input SUT is removed through a digital filter with bandwidth $B_e = 125$ MHz.

of the sampling pulse. For example, a 2.5 ps (FWHM) pulse requires a dispersion mismatch below $\Delta\ddot{\phi} \leq 2.24\,\mathrm{ps}^2\,\mathrm{rad}^{-1}$, which is roughly the equivalent to 100 meters of standard SMF.

It is also important to mention that when dealing with short sampling pulses (i.e., with bandwidths spanning several hundreds of GHz), TOD may not be negligible. In the temporal Talbot effect, TOD induces temporal distortions that may impede the formation of perfect self-images.[51] An example of this are the pulse-to-pulse amplitude fluctuations observed in the sampling pulse train in Figure 4, which represents an additional source of distortion impacting the SUT. Although the subsequent decimation process will alleviate the effect of these fluctuations, a smart selection of the POD parameters is important to minimize the impact of TOD effects. On one hand, a wise approach to designing the POD parameters involves selecting the lower GVD value from the two choices presented in Equations 2–3. This not only minimizes GVD but also results in a reduced TOD. On the other hand, one can use specially tailored chirped fiber Bragg gratings (CFBGs) with low high-order dispersion terms. Alternatively, by properly concatenating optical fibers with opposite β_3, TOD can be completely eliminated, thus realizing perfect temporal self-images, as it was recently demonstrated in ref. [52]. Regarding the practical implementation of the GVD stages, alternative de-

vices to optical fibers can be used. For instance, widely employed CFBG can be designed to provide an accumulated GVD equivalent to hundreds of km of standard single-mode optical fiber with much lower insertion losses. Also, novel on-chip discrete phase filter designs providing large amounts of GVD[53] are a very promising path toward the integration of the POD in a single chip.

Another important practical consideration concerns the polarization state of the incoming SUT. Polarization alignment is crucial for the efficient realization of the parametric oversampling process, and in many practical applications, the incoming signal's polarization state may not be known and/or it may change over time. To address this issue, a polarization-insensitive POD processor can be implemented by utilizing techniques similar to those already demonstrated in the context of FOPAs[54,55] and FWM-based time-lens systems.[56] For instance, this would only involve replacing the nonlinear medium in Figure 2a with a nonlinear loop constructed by a polarization beam splitter, where the pump pulse train is equally split into two orthogonal polarization components before being coupled into the nonlinear loop. In this way, the SUT is split into its two orthogonal polarizations. By doing so, the parametric oversampling occurs equally over the two polarization components.

Another important feature to be noted is that although here we demonstrated the oversampling-and-decimation concept on intensity-modulated signals, the POD output preserves the full complex information of the original SUT, in both magnitude and phase (though conjugated, as per the features of the generated idler). Only in the case of fractional decimation factors, a residual pulse-to-pulse phase modulation will be present. Such phase can be well determined and, thus, can be further removed. Consequently, the proposed method could be used to improve the detection accuracy of signals in which the relevant information is also contained in the phase, for example, for communication data signals with complex modulation formats such QAM.

In summary, we have proposed a novel photonic signal processing concept consisting in parametric-assisted oversampling followed by lossless decimation. We have experimentally demonstrated the realization of integer (even and odd) as well as fractional decimation factors. In this work, we applied this concept for the simultaneous waveform amplification and wavelength-agnostic mitigation of noise in optical signals. The proposed scheme integrates the FWM-based parametric amplification with the decimation-based passive amplification, where we demonstrated peak-to-peak amplification of GHz-bandwidth signals by a factor ≈ 50. The all-optical nature of the POD enabled us to reach a (sampling rate)×(passive amplification factor) exceeding 380 GHz -with potential to reach the THz regime-, which is more than an order of magnitude improvement versus electro-optic implementations of Talbot-based amplifiers. By achieving ultrahigh decimation factors (> 750) we demonstrated subnoise recovery of narrowband optical signals, fairly outperforming conventional methodologies based on direct detection combined with optical and digital filtering. Besides the recovery of noise-dominated optical signals demonstrated here, we foresee the potential of the oversampling and decimation processes for a wide range of applications across different fields, like photonic-assisted ADCs, photonics computing and neural networks.

Supporting Information

Supporting Information is available from the Wiley Online Library or from the author.

Acknowledgements

Conflict of Interest

The authors declare no conflict of interest.

Data Availability Statement

The data that support the findings of this study are available from the corresponding author upon reasonable request.

Keywords

[1] E. Agrell, M. Karlsson, A. Chraplyvy, D. J. Richardson, P. M. Krummrich, P. Winzer, K. Roberts, J. K. Fischer, S. J. Savory, B. J. Eggleton, M. Secondini, F. R. Kschischang, A. Lord, J. Prat, I. Tomkos, J. E. Bowers, S. Srinivasan, M. Brandt-Pearce, N. Gisin, *J. Opt.* **2016**, *18*, 063002.
[2] D. Solli, J. Chou, B. Jalali, *Nat. Photonics* **2008**, *2*, 48.
[3] M. Liebel, C. Toninelli, N. F. van Hulst, *Nat. Photonics* **2018**, *12*, 45.
[4] J. Capmany, D. Novak, *Nat. Photonics* **2007**, *1*, 319.
[5] D. Marpaung, C. Roeloffzen, R. Heideman, A. Leinse, S. Sales, J. Capmany, *Laser Photonics Rev.* **2013**, *7*, 506.
[6] A. S. Daryoush, in *Microwave Photonics*, Wiley **2009**, pp. 239–289.
[7] Y. He, K. G. Baldwin, B. J. Orr, R. B. Warrington, M. J. Wouters, A. N. Luiten, P. Mirtschin, T. Tzioumis, C. Phillips, J. Stevens, B. Lennon, S. Munting, G. Aben, T. Newlands, T. Rayner, *Optica* **2018**, *5*, 138.
[8] P. Dong, Q. Chen, *LiDAR remote sensing and applications*, CRC Press, Boca Raton **2017**.
[9] Y. Lu, T. Zhu, L. Chen, X. Bao, *J. Lightwave Technol.* **2010**, *28*, 3243.
[10] G. P. Agrawal, *Lightwave Technology: Telecommunication Systems*, John Wiley & Sons, Hoboken **2005**.
[11] T. Torounidis, P. A. Andrekson, B.-E. Olsson, *IEEE Photonics Technol. Lett.* **2006**, *18*, 1194.
[12] A. Peric, S. Moro, N. Alic, A. J. Anderson, C. McKinstrie, S. Radic, in *Proc. Frontiers in Optics 2010/Laser Science XXVI*, Optica Publishing Group, **2010**.
[13] J. M. C. Boggio, S. Moro, E. Myslivets, J. R. Windmiller, N. Alic, S. Radic, *IEEE Photonics Technol. Lett.* **2009**, *21*, 612.
[14] V. Gordienko, M. Stephens, A. El-Taher, N. Doran, *Opt. Express* **2017**, *25*, 4810.
[15] P. O. Hedekvist, M. Karlsson, P. A. Andrekson, *J. Lightwave Technol.* **1997**, *15*, 2051.
[16] S. Zlatanovic, J. S. Park, S. Moro, J. M. C. Boggio, I. B. Divliansky, N. Alic, S. Mookherjea, S. Radic, *Nat. Photonics* **2010**, *4*, 561.
[17] E. Temprana, V. Ataie, A. Peric, N. Alic, S. Radic, in *Proc. Optical Fiber Communication Conference*, Optical Society of America, **2014**, Th1H.2.
[18] P. A. Andrekson, M. Westlund, *Laser Photonics Rev.* **2007**, *1*, 231.
[19] M. A. Foster, R. Salem, D. F. Geraghty, A. C. Turner-Foster, M. Lipson, A. L. Gaeta, *Nature* **2008**, *456*, 81.
[20] C. Zhang, J. Xu, P. Chui, K. K. Wong, *Sci. Rep.* **2013**, *3*, 1.
[21] E. Desurvire, M. N. Zervas, *Phys. Today* **1995**, *48*, 56.
[22] P. A. Andrekson, M. Karlsson, *Adv. Opt. Photonics* **2020**, *12*, 367.
[23] Z. Ye, P. Zhao, K. Twayana, M. Karlsson, V. Torres-Company, P. A. Andrekson, *Sci. Adv.* **2021**, *7*, 38.
[24] M. E. Marhic, *Fiber optical parametric amplifiers, oscillators and related devices*, Cambridge University Press, Cambridge **2008**.
[25] J. Hansryd, F. Dross, M. Westlund, P. Andrekson, S. Knudsen, *J. Lightwave Technol.* **2001**, *19*, 1691.
[26] M. A. Foster, A. C. Turner, J. E. Sharping, B. S. Schmidt, M. Lipson, A. L. Gaeta, *Nature* **2006**, *441*, 960.
[27] F. Shen, A. Wang, *Appl. Opt.* **2005**, *44*, 5206.
[28] W. Wei, L. Yi, Y. Jaouën, W. Hu, *Opt. Express* **2014**, *22*, 23249.
[29] C. Porzi, G. J. Sharp, M. Sorel, A. Bogoni, *IEEE J. Quantum Electron.* **2019**, *56*, 1.
[30] A. Choudhary, Y. Liu, D. Marpaung, B. J. Eggleton, *IEEE J. Sel. Top. Quantum Electron.* **2018**, *24*, 1.
[31] S. J. Savory, *IEEE J. Sel. Top. Quantum Electron.* **2010**, *16*, 1164.
[32] R. N. McDonough, A. D. Whalen, *Detection of signals in noise*, Academic Press, Cambridge **1995**.
[33] R. Maram, J. Van Howe, M. Li, J. Azaña, *Nat. Commun.* **2014**, *5*, 1.
[34] R. Maram, M. Seghilani, J. Jeon, X.-Z. Li, L. Romero-Cortés, J. Van Howe, J. Azaña, *IEEE Photonics Technol. Lett.* **2018**, *30*, 665.
[35] C. R. Fernández-Pousa, R. Maram, J. Azaña, *Opt. Lett.* **2017**, *42*, 2427.
[36] M. P. Fernández, L. Romero-Cortés, S. R. Konatham, B. Crockett, L. A. Bulus-Rossini, P. A. Costanzo-Caso, J. Azaña, *Opt. Lett.* **2020**, *45*, 3557.

[37] B. Crockett, L. Romero-Cortés, R. Maram, J. Aza na, *Optica* **2022**, *9*, 130.

[38] M. W. Hauser, *J. Audio Eng. Soc.* **1991**, *39*, 3.

[39] B. Leung, *Analog Integr. Circuits Signal Process* **1991**, *1*, 65.

[40] T. Jannson, J. Jannson, *JOSA* **1981**, *71*, 1373.

[41] J. Azaña, M. A. Muriel, *IEEE J. Sel. Top. Quantum Electron.* **2001**, *7*, 728.

[42] M. V. Berry, S. Klein, *J. Mod. Opt.* **1996**, *43*, 2139.

[43] L. Romero Cortés, R. Maram, H. Guillet de Chatellus, J. Azaña, *Laser Photonics Rev.* **2019**, *13*, 1900176.

[44] L. Romero-Cortés, H. G. de Chatellus, J. Azaña, *Opt. Lett.* **2016**, *41*, 340.

[45] R. E. Crochiere, L. R. Rabiner, *Proc. IEEE* **1981**, *69*, 300.

[46] L. Tan, J. Jiang, *Digital signal processing: fundamentals and applications*, Academic Press, Cambridge **2018**.

[47] R. Salem, M. A. Foster, A. L. Gaeta, *Adv. Opt. Photonics* **2013**, *5*, 274.

[48] R. Stolen, J. Bjorkholm, *IEEE J. Quantum Electron.* **1982**, *18*, 1062.

[49] J. Hansryd, P. A. Andrekson, M. Westlund, J. Li, P.-O. Hedekvist, *IEEE J. Sel. Top. Quantum Electron.* **2002**, *8*, 506.

[50] G. P. Agrawal, In *Nonlinear Science at the Dawn of the 21st Century*, Springer, New York, **2000**, pp. 195–211.

[51] J. Fatome, S. Pitois, G. Millot, *Opt. Commun.* **2004**, *234*, 29.

[52] Y. Zhao, L. Chen, W. Wang, R. Wang, H. Hu, X. Wang, C. Zhang, W. Zhang, X. Zhang, *APL Photonics* **2020**, *5*, 046102.

[53] S. Kaushal, J. Azaña, *Opt. Lett.* **2020**, *45*, 4603.

[54] K. K. Wong, M. E. Marhic, K. Uesaka, L. G. Kazovsky, *IEEE Photonics Technol. Lett.* **2002**, *14*, 1506.

[55] C. B. Gaur, F. Ferreira, V. Gordienko, V. Ribeiro, Á. D. Szabó, N. J. Doran, *Opt. Express* **2020**, *28*, 19362.

[56] S. Wang, X. Dong, B. Li, K. K. Wong, *Opt. Lett.* **2021**, *46*, 5627.